Synergistic adsorption of lanthanum ions and fatty acids for efficient rare-earth phosphate recovery: Surface analysis and ab initio molecular dynamics studies

A. Geneyton, Y. Foucaud, L.O. Filippov, N.-E. Menad, A. Renard, M. Badawi

A. Geneyton : Conceptualization, Methodology, Validation, Investigation, Formal analysis, Visualization, Writing- Original draft preparation, Writing- Reviewing and Editing. Y. Foucaud : Conceptualization, Methodology, Validation, Investigation, Formal analysis, Visualization, Writing- Original draft preparation, Writing- Reviewing and Editing. L.O. Filippov : Conceptualization, Resources, Writing- Reviewing and Editing, Supervision, Project administration, Funding acquisition. N. E Menad : Conceptualization, Resources, Writing- Reviewing and Editing, Supervision, Project administration, Funding acquisition. A. Renard : Investigation, Formal analysis, Resources. M. Badawi : Conceptualization, Formal analysis, Resources, Writing- Original draft preparation, Writing- Reviewing and Editing, Supervision.

Declaration of interests

☒ The authors declare that they have no known competing financial interests or personal relationships that could have appeared to influence the work reported in this paper.

☐The authors declare the following financial interests/personal relationships which may be considered as potential competing interests:

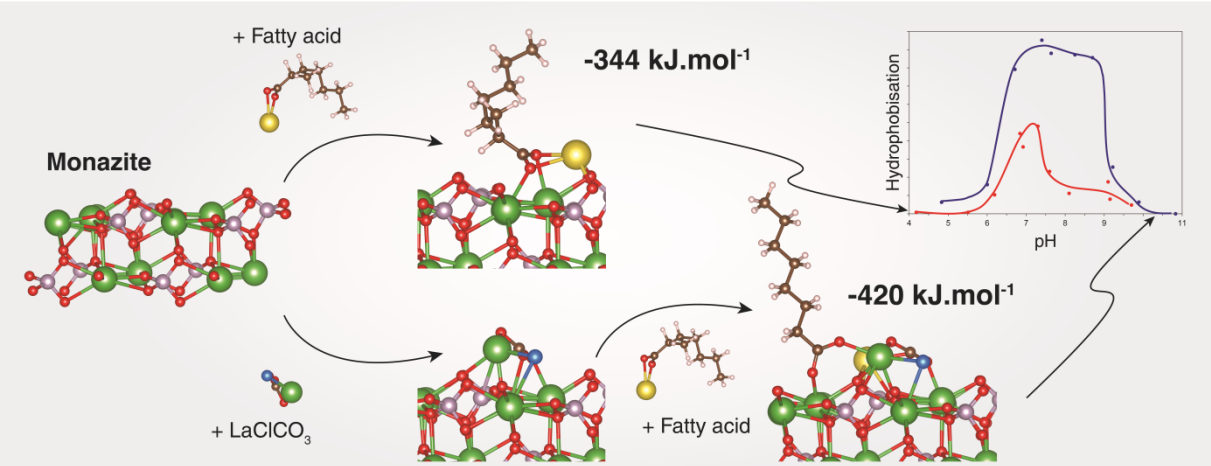

- Effect of lanthanum chloride addition on monazite floatability was investigated
- Lanthanum ions adsorb strongly on the phosphate groups of the monazite surface
- Lanthanum cations increase the adsorption energy of the carboxylate collectors
- When $LaCl_3$ is used, the monazite hydrophobization by fatty acids is improved
- Combination of LaCl3 and fatty acids enhances the recovery of rare-earth by flotation

Synergistic adsorption of lanthanum ions and fatty acids for efficient rare-earth phosphate recovery: surface analysis and *ab initio* molecular dynamics studies

A. Geneyton[a,b,l] ,Y. Foucaud[a,l], L.O. Filippov[a,e*], N.-E Menad[b], A. Renard[d], M. Badawi[c*]

[a]Université de Lorraine, CNRS, GeoRessources, F- 54000 Nancy, France

[b]BRGM, Water, Environment, Processes and Analysis Department, Waste and Raw Materials & Recycling Unit, 3 Avenue Claude Guillemin, BP 36009, 45060 Orléans Cedex, France

[c]Université de Lorraine, CNRS, LPCT, F- 54000 Nancy, France

[d]Université de Lorraine, CNRS, LCPME, F- 54000 Nancy, France

[e]National University of science and technology MISIS, Leninsky pr., 4, 119049 Moscow, Russia

[l] These authors contributed equally.

*Corresponding authors: lev.filippov@univ-lorraine.fr; michael.badawi@univ-lorraine.fr

Abstract

Rare earth elements (REEs) are indispensable in our daily life but they naturally occur in minerals, which are generally difficult to concentrate by the froth flotation method. Considering the significant affinity of lanthanum ions for phosphate species as well as for carboxylate groups, the influence of a lanthanum salt ($LaCl_3$) on the adsorption of carboxylate species on monazite surface [$(La,Ce,Nd)PO_4$] was investigated by bubble/particle adhesion tests, X-ray photoelectron spectroscopy (XPS), and atomistic simulations based on density functional theory (DFT). Both theoretical and experimental results demonstrated that lanthanum ions adsorb on the phosphate groups of monazite surface under the $LaClCO_3$ form with a significant adsorption energy. Also, the hydrophobization of the monazite surface with fatty acids is considerably improved in presence of $LaCl_3$, which is in accordance with DFT calculations: the lanthanum ions pre-adsorbed on monazite surface act as highly attractive adsorption sites for carboxylate collectors. In particular, these bridging cations significantly increase the adsorption energy of carboxylate collectors, from 344 to 420 $kJ{\cdot}mol^{-1}$ in absolute value. This synergistic adsorption will allow developing new methods for efficient monazite recovery from complex ores, a promising step for the recovery of critical raw materials.

Keywords: Flotation; Monazite; Lanthanum chloride; Carboxylate; Activation; DFT

1. Introduction

The world demand for rare earth elements (REE) has considerably increased over the past few years, mostly to produce permanent magnets that support the energy transition, in particular the development of renewable electricity production and the growing demand for electric vehicles. The production of light REEs, mainly used for these applications, is currently largely dominated by the exploitation of a few massive carbonatite-related deposits, which results in a supply chain risk for importing countries. In the above-mentioned ores, REE-bearing minerals (REM) are exclusively concentrated through the froth flotation method. REM flotation is generally achieved with deprotonated carboxylic or hydroxamic acids [1–3], also named carboxylates and hydroxamates, respectively. These chemical reagents, so-called collectors, adsorb on REM surfaces and make them hydrophobic, which allows the air bubbles rising in the flotation machine to collect REM particles in the froth. The flotation selectivity directly arises from the difference in the affinity of these surfactants for REM surfaces and for gangue mineral surfaces. Therefore, low REM grades as well as the presence of certain gangue minerals can result in lower amounts of collector adsorbed on REM surfaces.

The fact that the bulk of light REE production is carried on by only a few massive exploitations, notably in China, is frequently contested on the view of the supply chain risk for importing countries. Many REE deposits and occurrences have also been identified all around the world albeit they have been classified as noneconomic primary or secondary sources considering the current economic context and the REM flotation practices. In particular, mine tailings can contain significant amounts of REEs [4–7] although, compared to classical primary REE deposits, they commonly exhibit lower grades, finer liberation sizes, and/or more complex mineralogical associations. In most deposits, including mine tailings and secondary ores, REE are contained in monazite [$(La,Ce,Nd)PO_4$]. Hence, it is of paramount interest to develop new methods for monazite flotation since it could make the exploitation of such non-conventional deposits economically viable.

Many studies highlighted that metal cations affect the adsorption of carboxylates and hydroxamates collectors on various minerals by playing a role of a bridge between the mineral surface and the collector functional group [8–16]. Therefore, the combined use of the aforementioned collectors and a metal cation that display a high affinity for both the collector group(s) and the mineral surface group(s) represents an interesting approach to improve the monazite flotation performances. Although a few recent studies deal with the use of lead nitrate in combination with hydroxamates to improve the monazite flotation performances [14,17], this approach has been relatively unexplored and suited metal cations are yet to be identified.

Interestingly, free lanthanum ions are known to form complexes with carboxylate ligands due to their considerable affinity for those anions [18–21]. Consequently, carboxylates and carboxylic acids are studied and commercialized as extractants for REE solvent extraction [22–25] while carboxylic-acid-based ion-exchange resins can be used to entrap lanthanide elements [26]. Besides, lanthanum under various forms displays an excellent capacity to bind free phosphate species. Indeed, soluble lanthanum compounds are commonly used as phosphate precipitants for wastewater treatment and serum phosphate regulation [27–31], while sparingly soluble lanthanum compounds are used as phosphate sequestering solutions [30,32,33] and lanthanum-modified minerals are commercialized as phosphate-removing materials [34–36].

The affinity of lanthanum ions for both carboxylate groups and phosphate species suggests coupled interactions between lanthanum ions, the functional group of carboxylate flotation collectors, and the phosphate groups present on the surface of monazite. This study addresses the existence of synergistic effects between lanthanum ions and fatty acids (carboxylate collectors) that could promote the adsorption of these collectors on the monazite surface, increasing its hydrophobicity and thus the monazite floatability. This promoting effect of lanthanum ions on the floatability of monazite using carboxylate collectors is investigated in this work by a combination of experimental (adhesion tests and X-Ray photoelectron spectroscopy) and theoretical methods (density functional

theory calculations) since it successfully unraveled complex molecular mechanisms over the past decades [37–42].

2. Materials and methods

2.1. Synthetic monazite

Adhesion tests and XPS analyses were performed using a synthetic monazite, obtained by a thermal treatment of rhabdophane, i.e. hydrated cerium phosphate, supplied by Alfa Aesar (99% purity). Rhabdophane was first compacted into pellets using a cylindrical press, which applied a compaction pressure of 80 kg·cm^{-1}. Then, the pellets were thermally treated in an electric muffle furnace following the procedure detailed by Geneyton and co-workers [43]. XRD analyses confirmed that the obtained product was pure monazite-(Ce), which was then manually crushed in an agate mortar and screened to get a -315+125 µm powder used for the adhesion tests. A further pulverization of this powder, conducted for 2 h in an agate planetary ball mill was required to meet the material requirements for XPS analyses. Although natural monazite generally exhibits a complex lanthanide distribution, a lanthanum-free monazite-(Ce) was considered as a material of choice to study the interactions between carboxylate collectors and the monazite surface, including in presence of $LaCl_3$ since trivalent lanthanide substitutions in monazites do not affect significantly these interactions [44].

2.2. Reagents

For adhesion tests and XPS analyses, a sodium oleate ($C_{17}H_{33}COONa$) solution at 1 x 10^{-6} mol·L^{-1} was used. This solution was produced by treatment of oleic acid (99% purity, supplied by Alfa Aesar) with sodium hydroxide (NaOH) in deionized water (18.2 MΩ·cm) at 60°C for 30 min. For some tests, before dilution, the sodium oleate solution was premixed with the same volume of lanthanum chloride ($LaCl_3$) solution at 1 x 10^{-3} mol·L^{-1}, produced by dissolution of hydrated $LaCl_3$ salt (99% purity,

supplied by Alfa Aesar), in deionized water. This $LaCl_3$ solution was also used alone to investigate the adsorption of lanthanum species on monazite surface.

2.3. Bubble/particle low-energy adhesion tests

The hydrophobicity of monazite grains surface, after treatment with solutions at low sodium oleate concentration, was studied by measuring the average number of grains attached to a bubble that was put in contact with a particle bed. The tests comprised a series of low-speed contacts between a still bubble and a mobile particle bed. Since the bubble remained perfectly still, stable adhesion occurred when the adhesion energy was high enough to lift a coarse particle (-315+125 µm) and, mostly, to resist the friction between the attached particle and the particles constituting the particle bed.

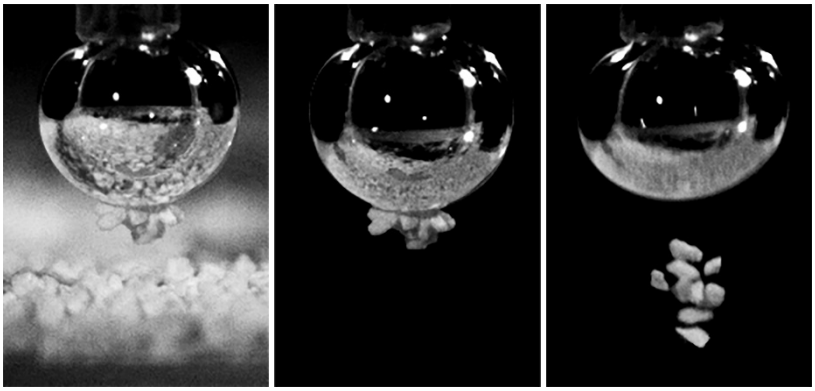

Fig. 1: Measure of the number of particles collected (bubble load) by putting the air bubble in contact with the particle bed (left), lowering the particle bed (middle), and detaching the attached particles by shocking while counting using a high-speed camera (right).

Prior to the adhesion tests, the treatment solution was prepared with its pH adjusted using NaOH or hydrochloric acid (HCl) at 0.1%, and was then placed in a closed test tube along with 100 mg of (-315+125 µm) synthetic monazite-(Ce) grains. After 24 h of treatment with no stirring, the particles were extracted with roughly 7 mL of solution and transferred to a glass cuvette to form a particle bed. A bubble with a diameter of 1.5 mm was generated and the particle bed was lifted using a micro-translation stage, to enable the contact with the bubble. After a contact time of 20 s, the

particle bed was smoothly moved down and a shock was applied on the bubble holder to detach the collected particles and to count them using a high-speed camera (Fig. 1). The bubble load was averaged from 25 adhesion tests for each investigated experimental condition.

2.4. X-Ray photoelectron spectroscopy (XPS)

The X-ray photoelectron spectra were recorded using a Kratos Axis Ultra DLD spectrometer (Kratos Analytical, U.K.) equipped with a monochromatic Al Kα X-ray source (1486.6 eV) operated at 120 W. Calculations of XPS elemental compositions were performed using the Kratos Vision 2.2.11 software package including the subtraction of Shirley-type background [45]. For XPS analyses, 100 mg of monazite powder was treated for 30 min in a beaker containing 50 mL of the $LaCl_3$ solution. Before and during this treatment, the pH was maintained constant at 8.5, a conventional pH for monazite flotation, using NaOH. The particles were then recovered by filtration through a nylon filter (0.8 µm pore size) and thoroughly rinsed with deionized water. The obtained powders were then placed in a desiccator under partial vacuum for soft drying prior to their introduction in the spectrometer.

2.5. DFT calculations

2.5.1. *Protocol of modeling and calculation settings*

The adsorption configurations and energies of species on the (100) monazite surface were determined through DFT calculations using the Vienna Ab initio Simulation Package VASP [46]. First, for each system, *ab initio* molecular dynamics (AIMD) simulations were carried out during 20 picoseconds to find the area of the phase space accessible at 300 K, *i.e.* the atoms positions that corresponded to a plausible initial condition for a subsequent geometry optimization. For AIMD simulations, a Nosé-Hoover thermostat was employed to set the temperature to 300 K with a time step of 1 fs.

Then, on this system, a DFT relaxation was performed until all forces were smaller than 0.01 $eV \cdot Å^{-1}$ to calculate the energy of the system and the corresponding contribution of dispersion energy.

The combination of AIMD simulations (at 300 K) with subsequent DFT calculations provided the most stable configurations efficiently as well as the adsorption energies with high accuracy. For each system, the adsorption energy was determined by subtracting the calculated energies of the isolated molecule and the isolated surface to the energy of the system where the molecule is adsorbed on the surface.

The following settings have been applied for both AIMD and DFT relaxations. The PAW method [47,48] with a plane wave cut-off energy of 450 eV was employed as well as the PBE functional [49] with the D2 correction to account for dispersion forces [50]. The Kohn-Sham equations [51] were solved self-consistently [52] until the energy difference between the cycles became lower than 10^{-8} eV. All the calculations were performed using the Γ-point only due to the large size of the cells.

2.5.2. *Structural Model*

First, a primitive cell of $LaPO_4$ was generated [53], fully relaxed, and used to create a (100) surface, which represents the most exposed surface for $LaPO_4$ [54–56]. This slab was then expanded to obtain a supercell containing 96 atoms (16 La, 16 P, and 64 O) which comprised two layers of eight lanthanum atoms associated with eight phosphate groups. The lattice parameters of this supercell were a = 6.8313 Å, b = 13.8476 Å, and c = 13.1561 Å. The crystal structure of monazite, shown in Fig. 2, consists of an alternation of nine-coordinated lanthanide ions (in enneaoxide polyhedrons) and four-coordinated phosphorus ions (in phosphate tetrahedrons). Three oxygen atoms of the phosphate group are three-coordinated (bonded to two lanthanum and the phosphorus) while the fourth is three-coordinated (bonded to three lanthanum and to the phosphorus). On the (100) surface, half of lanthanum ions are seven-coordinated and the other half are eight-coordinated whereas, in the $LaPO_4$ bulk, lanthanum ions are nine-coordinated (Fig. 2). A vacuum of 15 Å was set between the uppermost atom, including the added molecules, and the upper limit of the cell following the a-axis (leading to c = 28.1561 Å) to avoid any unwanted interaction due to the cell

periodicity. For all the calculations, atoms in the bottom layer of the slab were frozen to their bulk positions.

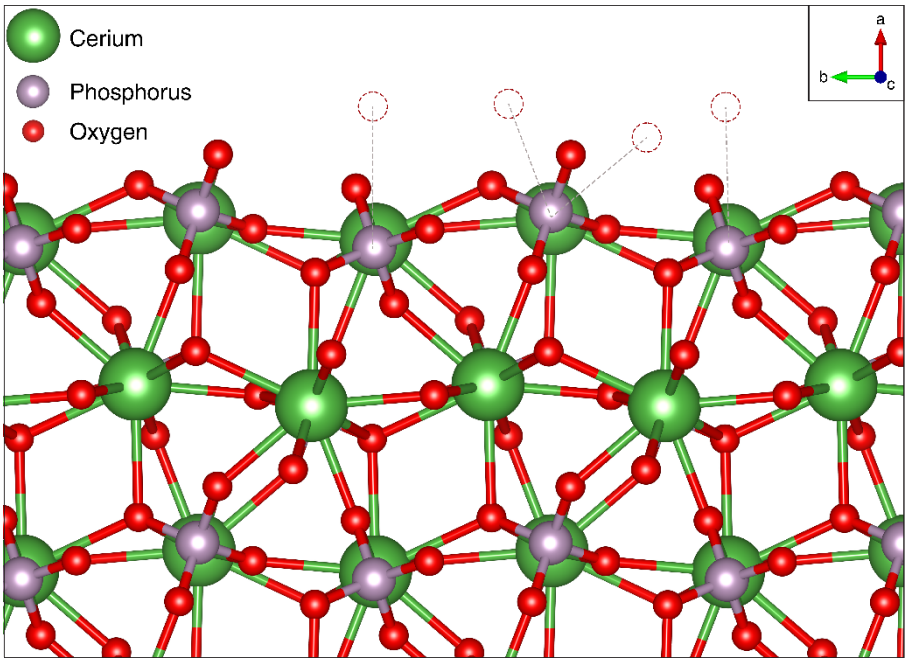

Fig. 2: Side view of the monazite-(Ce) (100) facet with highlighted surface oxygen atoms under-coordinations, viewed using the VESTA program **[57]**. *The crystallographic axes are indicated by the arrows at the top right of the figure.*

3. Results and discussion

3.1. Affinity of lanthanum ions for monazite surface

Lanthanum ions are known to have a strong affinity for free phosphate species present in bulk solution [28–30]. Hence, it suggests a significant binding ability between lanthanum ions and the lattice phosphate groups exposed to the solution, owing to their under-coordinated oxygen atoms. However, although the oxygen atoms of the lattice phosphate tetrahedrons are under-coordinated on the cleaved monazite surface, their electrons excesses are intrinsically lower than those of the oxygen atoms of free phosphate species. Therefore, the adsorption of lanthanum ions on the oxygen atoms of the monazite surface phosphate groups had yet to be proven. XPS analyses were then performed to determine whether lanthanum ions interact with the surface phosphate groups, as it

was assumed. The semi-quantitative XPS-determined surface atomic compositions of monazite-(Ce) treated with different $LaCl_3$ concentrations are presented in Table 1.

Table 1: Composition of the monazite surface after treatment in $LaCl_3$ solutions at various concentrations (expressed in atomic per cent). n.d. = the content of the element is below the detection limit.

$LaCl_3$ dosage	Composition (at.%)						
	Ce	La	O	CO_3 species	C species	P	Cl
0 mol L^{-1}	13.4 %	n.d.	49.4 %	1.3 %	24.4 %	11.6 %	n.d.
1.10^{-5} mol L^{-1}	11.8 %	0.6 %	47.0 %	1.6 %	28.3 %	10.8 %	n.d.
1.10^{-4} mol L^{-1}	11.7 %	2.9 %	49.5 %	1.8 %	23.2 %	10.3 %	0.6 %
1.10^{-3} mol L^{-1}	7.9 %	5.5 %	45.1 %	4.8 %	26.3 %	8.1 %	2.3 %

First, the amount of lanthanum ions identified on the mineral surface increases with the $LaCl_3$ concentration in solution, which means that lanthanum ions adsorb on the monazite surface (Table 1). Furthermore, carbonate species are significantly more present on the monazite surface when this mineral is treated in a solution at 1.10^{-3} mol·L^{-1} $LaCl_3$ compared to solutions with lower $LaCl_3$ concentrations (Table 1). Similarly, the amount of chlorine adsorbed on the mineral surface increases with the $LaCl_3$ concentration. Considering that the electro-neutrality of the mineral surface must be satisfied, the adsorption of lanthanum ions is necessarily accompanied by the adsorption of counter-ions. From a thermodynamic perspective, under the given physicochemical conditions (pH 8.5 and 1.10^{-3} mol·L^{-1} of $LaCl_3$), free lanthanum ions in solution react with carbonate ions to form $LaCO_3^+$ and $La(CO_3)_2^-$ species (Fig. 3), which probably adsorb on the mineral surface during this treatment. Hence, the above-mentioned increases in the chlorine, lanthanum, and carbonate amounts on the monazite surface can be explained by the adsorption of $LaCO_3Cl$ along with other species described on Fig. 3.

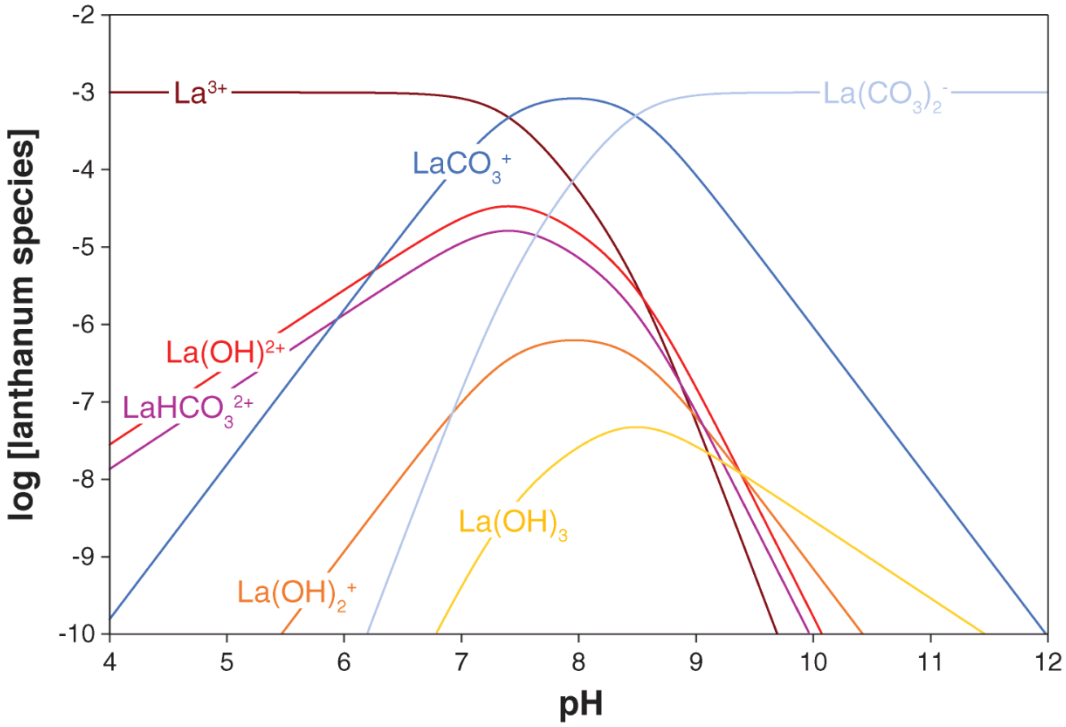

Fig. 3: Speciation diagram of lanthanum species in an aqueous solution equilibrated with the air, for a total lanthanum concentration of 1 x 10^{-3} mol·L^{-1}. *The thermodynamic constants used for this model are those used by Geneyton and co-workers* [58].

The high-resolution XPS core level spectra recorded after a treatment of monazite-(Ce) in solutions with different concentrations of $LaCl_3$ are presented in Fig. 4. First, no significant differences can be observed in the XPS Ce(3d) core level spectra of the different monazite-(Ce) powders (Fig. 4a). Besides, the variations in the intensity of the La(3d) spectra confirm the adsorption of lanthanum ions onto monazite surface (Fig. 4b) while the O(1s) core level spectra present a slight shift of about 0.25 eV towards higher binding energies when the monazite-(Ce) is treated with $LaCl_3$ solutions, regardless the concentration (Fig. 4c). Considering that the extent of this shift is equivalent whatever the amount of lanthanum adsorbed on the monazite surface, this could be interpreted as an artefact. However, though little significance, this result could also be related to the formation of La-O bonds (from $LaPO_4$) on the surface, which shifts the binding energy of O(1s) compared to Ce-O bonds (from $CePO_4$). Interestingly, while the peak attributed to adventitious carbon always presents the same binding energy (Fig. 4d), the peak assigned to carbonate species (around 289-290 eV) is shifted

towards higher binding energies with the increase of the $LaCl_3$ concentration in solution (Fig. 5). In a previous study, we demonstrated that, under the pH and conditions used for this treatment, carbonate species do not naturally adsorb on monazite surface [58]. Therefore, this shift probably results from the binding of carbonate ions with adsorbed lanthanum ions rather than with surface cerium ions, since these latter exhibit a lower electron vacancy regarding their coordination with lattice oxygen atoms (coordination number of seven or eight). However, this shift could also be related to an increase in the amount of hydrogen carbonate species adsorbed on the lanthanum-modified monazite surface: these ions have higher C(1s) binding energies compared to carbonate ions [59,60]. The P(2p) core level spectra display no variation with the $LaCl_3$ concentration (Fig. 4e), indicating no change in the close chemical environment of P atoms. The presence of chlorine atoms on the monazite-(Ce) surface (Fig. 4f) confirms the atomic quantifications (Table 1): in addition to carbonate ions, chloride ions also adsorb on the mineral surface to balance the lanthanum ions electrical charge.

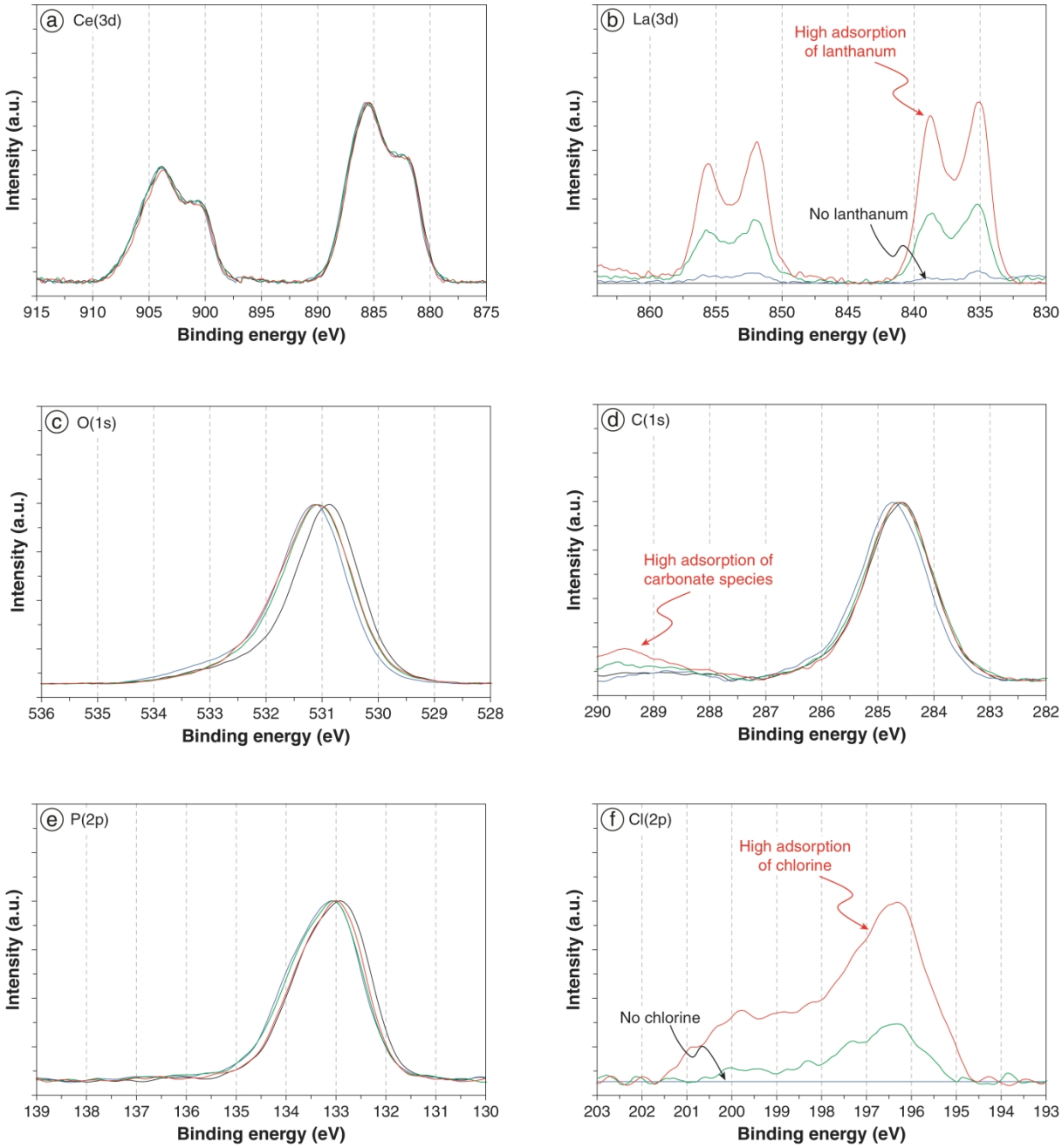
a Ce(3d)
Intensity (a.u.)
915 910 905 900 895 890 885 880 875
Binding energy (eV)
b La(3d)
High adsorption of lanthanum
No lanthanum
Intensity (a.u.)
860 855 850 845 840 835 830
Binding energy (eV)
c O(1s)
Intensity (a.u.)
536 535 534 533 532 531 530 529 528
Binding energy (eV)
d C(1s)
High adsorption of carbonate species
Intensity (a.u.)
290 289 288 287 286 285 284 283 282
Binding energy (eV)
e P(2p)
Intensity (a.u.)
139 138 137 136 135 134 133 132 131 130
Binding energy (eV)
f Cl(2p)
High adsorption of chlorine
No chlorine
Intensity (a.u.)
203 202 201 200 199 198 197 196 195 194 193
Binding energy (eV)
Monazite-(Ce) treated in absence of LaCl3
Monazite-(Ce) treated in 1x10-5 M LaCl3 solution
Monazite-(Ce) treated in 1x10-4 M LaCl3 solution
Monazite-(Ce) treated in 1x10-3 M LaCl3 solution

Fig. 4: High-resolution XPS La(3d) core level spectra and intensity-normalized Ce(3d), O(1s), C(1s), and P(2p) spectra of monazite after treatment in lanthanum chloride solutions.

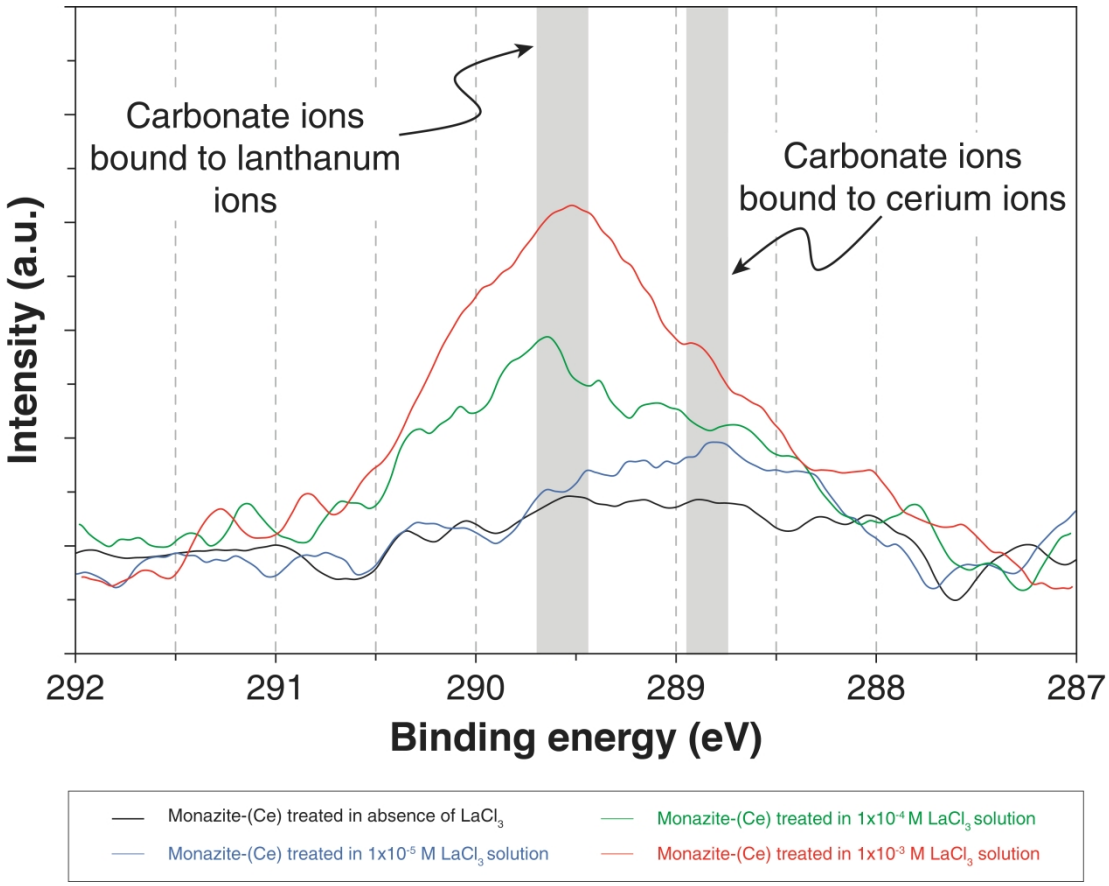

Fig. 5: Detailed view of the peak assigned to the carbonate species on the high resolution XPS C(1s) core level spectra. Shirley-type background was not subtracted to improve readability of the lateral shift.

DFT simulations were conducted to gain understanding in the molecular mechanisms involved in the adsorption of lanthanum species on the monazite surface. XPS results and thermodynamic calculations demonstrated the dominance of $LaCO_3^+$ over the other lanthanum species in solution as well as adsorbed on the monazite surface. This led us to investigate the adsorption of $LaCO_3^+$ through DFT calculations, which, however, required global electrical neutrality. To address this issue, a chloride atom was added close to the $LaCO_3^+$ molecule and the adsorption of $LaClCO_3$ species was considered in the calculations. After the AIMD simulation followed by a DFT relaxation (see Section 2.5.1 for the details of the modeling protocol), the lanthanum, chloride, and carbonate ions establish bonds with the monazite surface atoms (Fig. 6). In particular, the lanthanum ion is bonded to two

surface oxygen atoms (one mono-coordinated and one bi-coordinated), with La-O distances of 2.43 Å and 2.53 Å, respectively. Therefore, this simulation confirms that lanthanum ions adsorb on the monazite surface by establishing bonds with the under-coordinated oxygen atoms of the lattice phosphate groups exposed to the solution. Furthermore, the carbonate ion establishes two O-La bonds with two different surface lanthanum ions, corresponding to a bidentate binuclear configuration. It is also bonded to the lanthanum ion of the $LaClCO_3$ molecule (Fig. 6), while the chlorine ion adsorbs by establishing a Cl-La bond with a surface lanthanum ion. Overall, the $LaClCO_3$ molecule adsorbs on the (100) monazite surface with ΔE_{ads} = -416.7 kJ·mol^{-1} including ΔE_{disp} = -190.8 kJ·mol^{-1}.

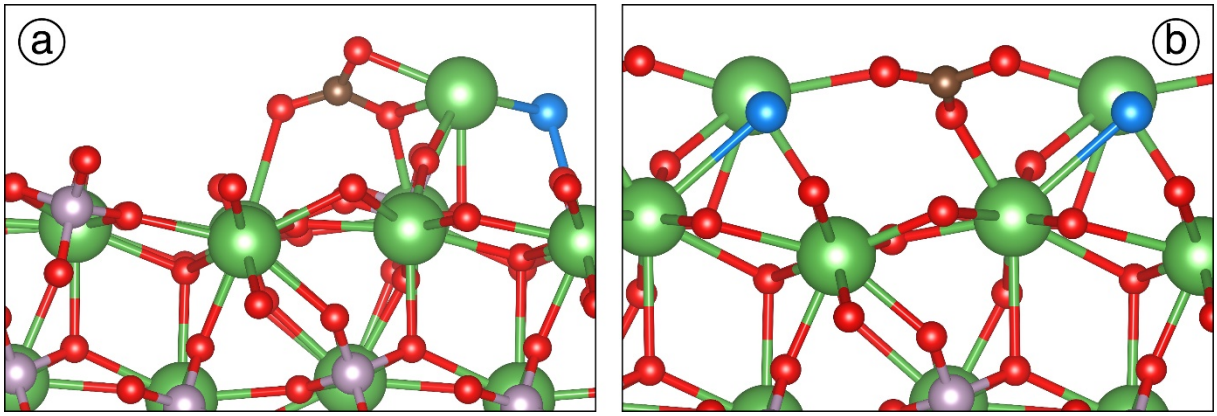

Fig. 6: Monazite surface with one $LaClCO_3$ molecule (a) and monazite surface fully coated with $LaClCO_3$ molecules (b) after 30 ps of AIMD simulation followed by a DFT relaxation. The green, red, light purple, blue, and brown balls represent lanthanum, oxygen, phosphorus, chlorine, and carbon atoms, respectively. The crystallographic orientation is the same than on Fig. 2.

Then, AIMD simulations were performed with more $LaClCO_3$ molecules on the monazite surface, *i.e.* with an increased surface coverage. The calculated adsorption energy per $LaClCO_3$ molecule, presented in Fig. 7, is similar for the adsorption of one and two $LaClCO_3$ molecules, which is consistent with the fact that they do not interact (large distance between them). For three $LaClCO_3$ molecules, the adsorption energy per molecule increases to -503.7 kJ·mol^{-1}·molecule^{-1}, which highlights the existence of intermolecular forces that favor the co-adsorption of $LaClCO_3$ on the (100) monazite surface. The addition of another $LaClCO_3$ molecule on the surface results in a decrease of

the global adsorption energy per molecule, which indicates a slight repulsion of the molecules and, thus, that a full coverage is reached. At high coverage, each lanthanum ion of $LaClCO_3$ molecules is bonded to three surface oxygen atoms from two different phosphate groups and the carbonate ions are bonded to two lanthanum ions from $LaClCO_3$ molecules (Fig. 6).

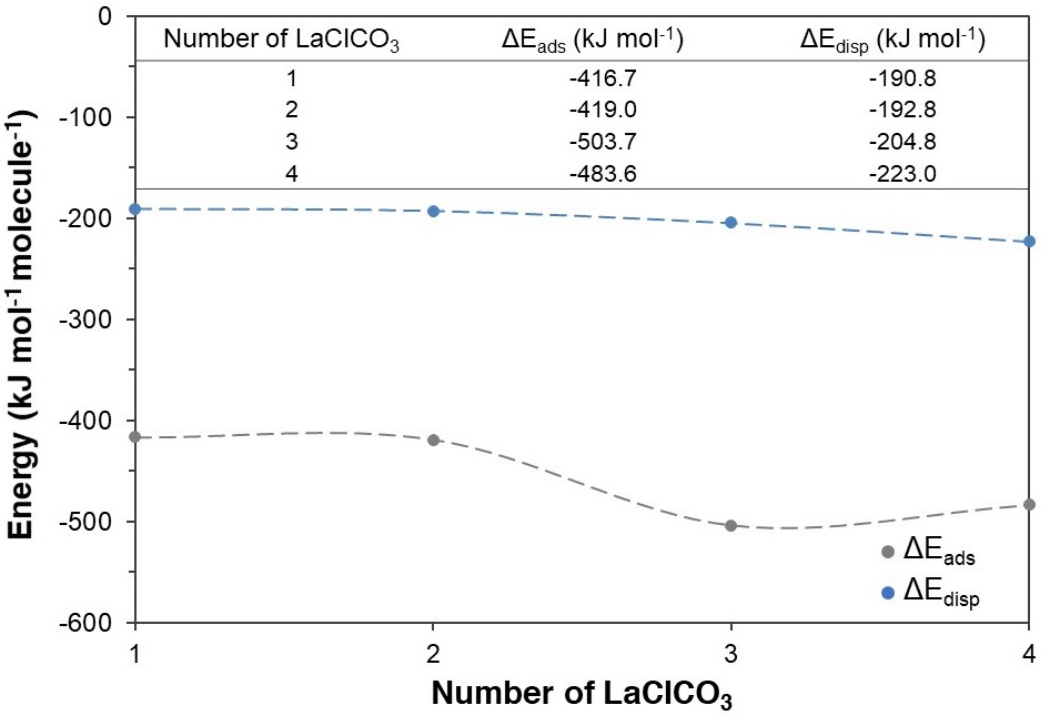

Fig. 7: Influence of the coverage of $LaClCO_3$ on the adsorption energy per $LaClCO_3$ molecule.

3.2. Influence of lanthanum ions on the adsorption of carboxylate collectors on the monazite surface

3.2.1. *Adhesion tests*

Two sets of adhesion tests were performed to determine if the presence of lanthanum ions in bulk solution influences the adsorption of sodium oleate on the monazite surface. In the first set, the monazite-(Ce) grains were treated in solutions that only contained sodium oleate while, in the second set, the monazite-(Ce) grains were treated with solutions that contained both sodium oleate and $LaCl_3$. The average number of monazite grains collected by a bubble is plotted as a function of the equilibrium pH in Fig. 8. The use of low amounts of lanthanum chloride significantly promotes the

adhesion of monazite grains over a wide pH range, which frequently results in the saturation of the bubble surfaces, as shown in Fig. 1. This enhanced hydrophobization of monazite surfaces in presence of $LaCl_3$ is probably related either to a stronger adsorption of sodium oleate on the monazite surface or to a better organization of the adsorption layer.

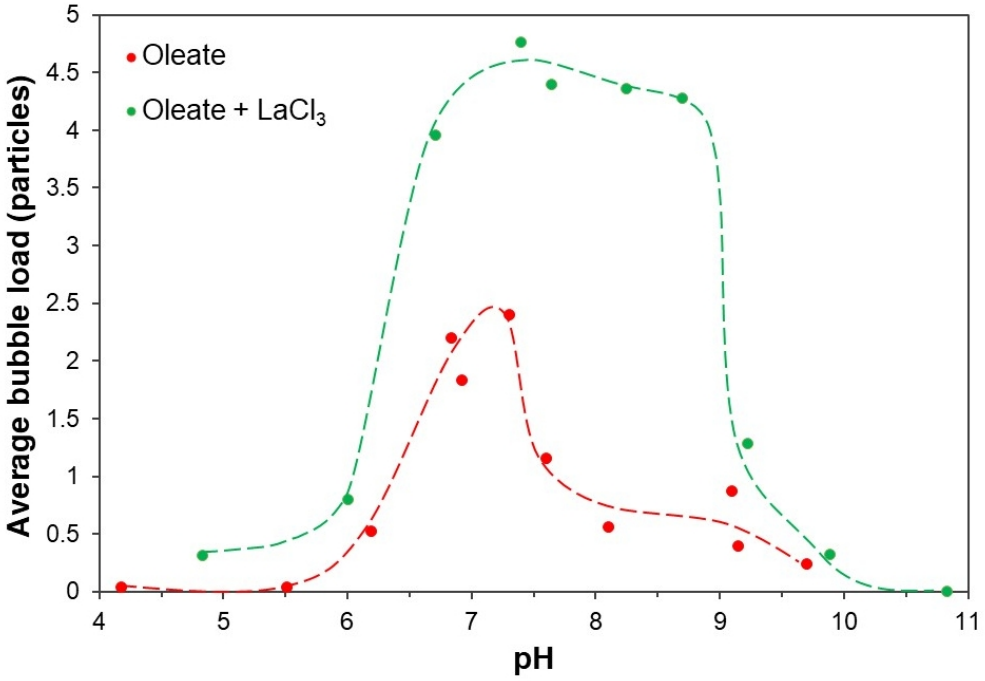

Fig. 8: Effect of lanthanum chloride on the number of monazite-(Ce) grains collected by a bubble

3.2.2. *DFT simulations*

In order to understand this experimental result, the adsorption of carboxylate collectors on the monazite surface was studied using DFT simulations. Considering the high computational costs induced by AIMD simulations, we choose the sodium octanoate molecule, *i.e.* with a chain that comprises only 8 carbon atoms, to represent the carboxylates commonly used in flotation. This assumption could be done since the polar group of the collectors mainly controls the interactions between the collector and the surface, probably responsible for the synergistic effects observed here, while the chain length is involved in the collector-collector co-adsorption processes. Moreover,

in a previous study, we demonstrated that the aliphatic chain length does not influence the configuration of the carboxylate functional group when it adsorbs onto semi-soluble mineral surfaces [61]. We also decided to not include water molecules in the simulations although the flotation process is performed in water. Very few studies investigated the hydration mechanisms of monazite albeit most sparingly soluble minerals are hydrated through molecular water physisorption [62–64]. The global objective of this study is to compare the adsorption of fatty acids onto a bare monazite surface and onto a monazite surface treated by $LaClCO_3$. Therefore, the water desorption or dehydroxylation process is strictly the same for the two cases and can be neglected for the comparison, albeit it will change the absolute values of ΔG. Three simulations were conducted to investigate the adsorption of a sodium octanoate molecule on the (100) monazite surface. The objective was to assess the influence of lanthanum chloride addition in flotation systems by determining the adsorption energies of the most favorable configuration for sodium octanoate on the bare and $LaClCO_3$-coated (100) monazite surfaces.

On the bare (100) monazite surface, sodium octanoate adsorbs by establishing La-O bonds between the two oxygen atoms of the carboxylate group and two surface lanthanum atoms, in a bidentate binuclear configuration (Fig. 9). The two La-O bonds are roughly equivalent, their lengths being 2.52 Å and 2.55 Å. Moreover, the two C-O bonds in the carboxylate group are strictly equivalent (d = 1.28 Å and d = 1.29 Å), confirming the electron delocalization due to the presence of the sodium atom in the vicinity of the carboxyl group. Indeed, during the DFT calculation, a valence electron is transferred from the sodium atom to the carboxyl group, which forms $R\text{-}COO^-$ and Na^+, the traditional species encountered in flotation systems. The sodium atom adsorbs on two surface oxygen atoms from two different phosphate groups, in the vicinity of the carboxylate group. Overall, sodium octanoate adsorbs with ΔE_{ads} = -343.5 kJ·mol^{-1} including ΔE_{disp} = -131.1 kJ·mol^{-1}, which is in moderate accordance with the -422 kJ·mol^{-1} reported in the literature [8].

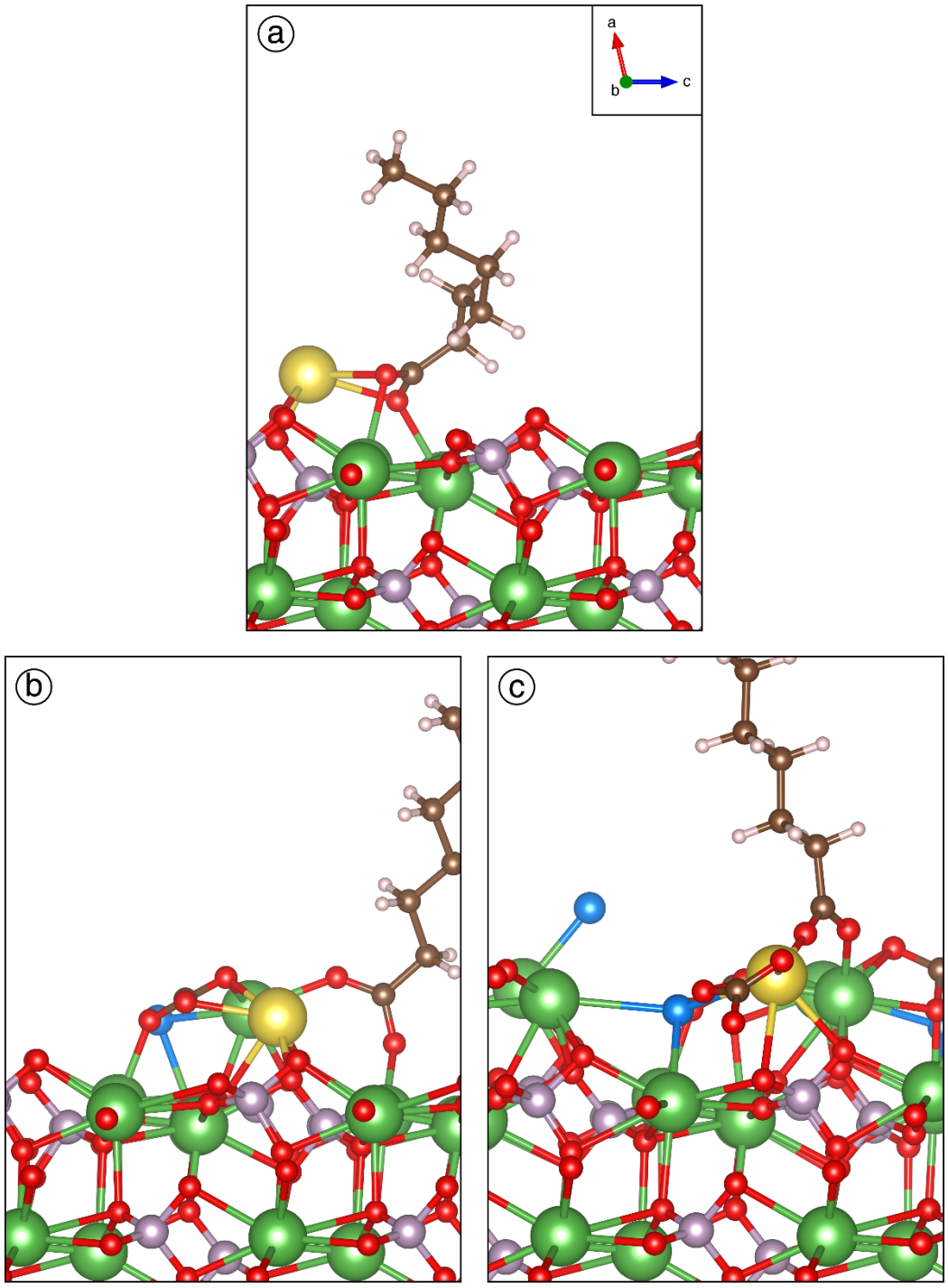

Fig. 9: Sodium octanoate adsorbed on bare monazite surface (a), monazite surface with one $LaClCO_3$ molecule (b), and monazite fully coated with $LaClCO_3$ (c) after 20 ps of AIMD simulation followed by a DFT relaxation. The green, red, light purple, blue, yellow, and brown balls represent lanthanum, oxygen, phosphorus, chlorine, sodium, and carbon atoms, respectively. The crystallographic axes are indicated for graph (a) and they are the same for the three graphs.

Besides, a similar simulation was conducted with a $LaClCO_3$ molecule previously adsorbed on the (100) monazite surface, placed in the fully relaxed configuration. Sodium octanoate adsorbs in a

bidentate binuclear mode by establishing a La-O bond with a surface lanthanum atom along with a La-O bond with the lanthanum atom of the $LaClCO_3$ molecule (Fig. 9). As previously, the two C-O bonds are strictly equivalent, with a bond length of 1.28 Å for both. The La-O bond between the surface lanthanum atom and the carboxylate oxygen atom is 2.50 Å long, which is similar to the adsorption of sodium octanoate on the bare surface. However, the La-O bond between the lanthanum of the $LaClCO_3$ molecule and the carboxylate oxygen atom is 2.37 Å long, which is significantly lower compared to lanthanum surface atoms. Consistently, the adsorption energy is also significantly higher in absolute value: when the $LaClCO_3$ molecule is pre-adsorbed, sodium octanoate adsorbs with ΔE_{ads} = -420.2 kJ·mol^{-1} including ΔE_{disp} = -118.7 kJ·mol^{-1}. This can explain the improvement of the monazite surface hydrophobicity when $LaCl_3$ is added prior to the collector addition, since its adsorption (under $LaClCO_3$ form) increases significantly the adsorption strength of the fatty acids on the monazite surface. Interestingly, the adsorption mechanisms are different on the monazite surface treated with $LaClCO_3$ compared to the bare surface: during the AIMD simulation, the sodium atom moves far from the octanoate (d>4.5 Å), which can be interpreted as an exchange between sodium atom and the lanthanum atom of the $LaClCO_3$ molecule.

3.2.3. *Structure of the adsorption layer*

Finally, the effect of the $LaCl_3$ concentration on the collector adsorption was assessed by adsorbing a sodium octanoate molecule onto a surface fully coated by $LaClCO_3$ molecules, *i.e.* with four molecules. In this configuration, the sodium octanoate adsorbs onto the $LaClCO_3$ layer by establishing a La-O bond between a lanthanum atom from $LaClCO_3$ layer and an oxygen atom of the carboxylate group. Also, it forms a Na-O bond while the sodium atom penetrates the $LaClCO_3$ layer to adsorb on a phosphate group of the monazite surface. The Na-O and La-O bond lengths are 2.23 Å and 2.25 Å, respectively, which is significantly lower compared to the surface with only one $LaClCO_3$ molecule or to the bare surface. Consistently, sodium octanoate adsorbs on the fully coated surface with ΔE_{ads} = -559.4 kJ·mol^{-1} including ΔE_{disp} = -29.9 kJ·mol^{-1}, which represents a very high adsorption energy in absolute value compared to the previous systems. Hence, it can be assessed that increasing the

$LaCl_3$ in the conditioning stage, *i.e.* increasing the $LaClCO_3$ coverage, will favor the adsorption of sodium octanoate in terms of adsorption energies. This crucial result demonstrates that the addition of $LaCl_3$ in the early stage of the flotation process affords an improved adsorption of fatty acids and could therefore lead to a better monazite recovery or a better flotation selectivity in favor of monazite. To complete this preliminary and promising finding, we also investigated the organization of the adsorption layer, and in particular the influence of $LaCl_3$ species ($LaClCO_3$ at pH 8.5) on it. Hence, additional atomistic simulations were performed with increasing sodium octanoate coverage on the surface with one $LaClCO_3$ and on the bare surface (Fig. 10). At low to moderate coverage, *i.e.* for 1-3 octanoate molecules, the adsorption energies per octanoate molecule are significantly higher in absolute value for the surface with a pre-adsorbed $LaClCO_3$. For 2 octanoates molecules, they do not interact with each other, which induce very similar adsorption energies per molecule than for a sole octanoate molecule. When the coverage increases, the adsorption energies per octanoate molecule become similar, indicating a low influence of the $LaClCO_3$ molecule on the surface. At high coverage, *i.e.* for 5-6 octanoate molecules, the molecular adsorption energies decrease in absolute values for both cases indicating that interactions between molecules and the surface become weaker, probably due to a significant polar repulsion between the carboxylate groups. Some artefacts can be present in Fig. 10, mainly due to the complex stabilisation of the aliphatic chains during the calculations and the initial locations of the sodium octanoate molecules on the surface. Therefore, the $LaClCO_3$ molecule adsorbed on the monazite surface does not significantly affect the organization of the adsorption layer. The adsorption of the first, second, and third carboxylate molecules is favored when a $LaClCO_3$ molecule is pre-adsorbed compared to the bare monazite surface. Consequently, the pre-adsorbed lanthanum ions constitute high activity adsorption sites on the monazite surface but do not control the tightness or the organization of the adsorption layer, which is mostly led by the packing area of the carboxylate species. Furthermore, the high coverages presented in Fig. 10 are probably never attained in realistic flotation systems since the formation of

an adsorption layer implies the maximisation of the lateral chain-chain interactions and the minimisation of the polar repulsion between the anionic groups.

Number of molecule(s)	ΔE_{ads} (kJ mol^{-1})		ΔE_{disp} (kJ mol^{-1})	
	Bare surface	Surface with $LaClCO_3$	Bare surface	Surface with $LaClCO_3$
1	-343.5	-420.2	-131.1	-118.7
2	-320.9	-452.3	-136.7	-212.9
3	-354.2	-417.7	-141.9	-203.3
4	-403.7	-351.7	-207.8	-144.0
5	-377.3	-363.6	-197.4	-157.5
6	-361.0	-345.1	-175.9	-145.7

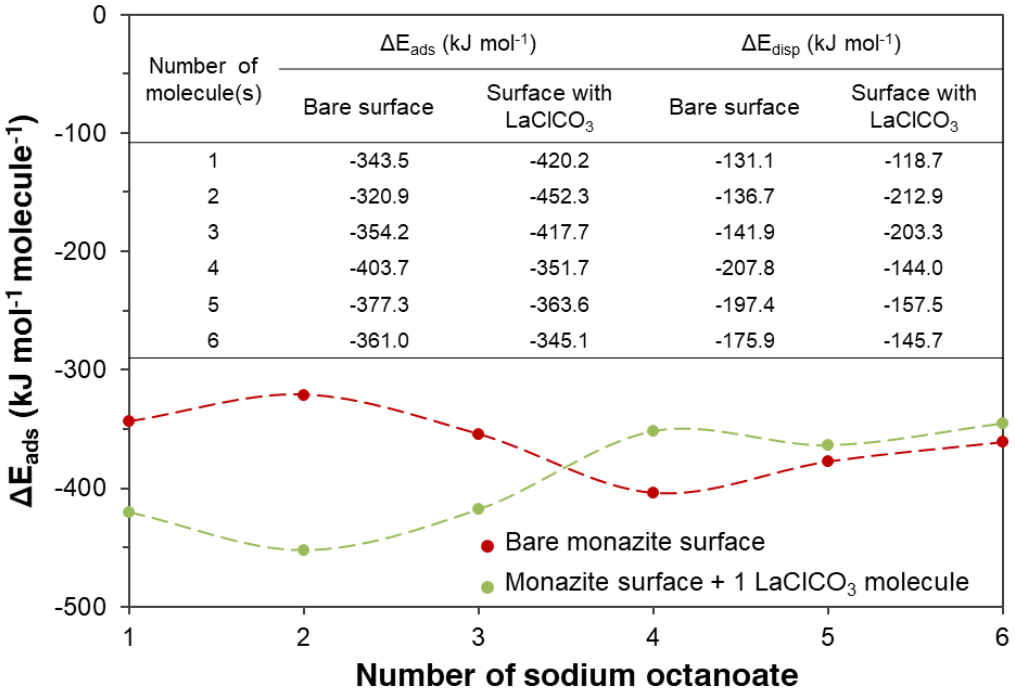

Fig. 10: Influence of the presence of one $LaClCO_3$ molecule on the monazite surface on the adsorption energy of sodium octanoate (adsorption energy per molecule)

4. Conclusion

In this work, we have investigated the existence of synergistic effects between carboxylate collectors and lanthanum ions to increase the monazite flotation performances, considering the high criticality of REEs. First, the affinity between lanthanum ions and the under-coordinated surface phosphate groups of a monazite-(Ce) was studied using XPS analyses and DFT simulations. XPS analyses confirmed that lanthanum ions adsorb on the monazite surface along with chloride and carbonate anions that act as counter-ions. Moreover, the DFT simulations performed in this work indicated that $LaClCO_3$ adsorbs onto monazite surface with ΔE_{ads} = -416.7 kJ·mol^{-1}, which illustrates the strong affinity existing between free lanthanum species and surface phosphate groups.

Besides, adhesion tests demonstrated that the hydrophobicity of a monazite-(Ce) surface is stronger when the mineral is conditioned in presence of $LaCl_3$ prior to sodium oleate compared to when it is conditioned with sole sodium oleate. The considerable synergistic effects existing between $LaCl_3$ and sodium oleate species were also highlighted by the DFT simulations, which were performed to investigate the adsorption of sodium octanoate on the monazite surface. The adsorption energies are significantly lower in absolute value when the collector is adsorbed on a bare monazite surface (-343.5 kJ mol^{-1}) rather than when the collector adsorbs on a bridging lanthanum cation (-420.2 kJ mol^{-1}). Furthermore, when the surface is completely coated by $LaClCO_3$ molecules, sodium octanoate adsorbs with ΔE_{ads} = -559.4 kJ mol^{-1}, which represents a significant value. Hence, the lanthanum ions, pre-adsorbed on the monazite surface, play an active role since they correspond to highly attractive adsorption sites for carboxylate collectors. However, they do not influence the organization and the tightness of the adsorption layer as increasing the coverage in terms of sodium octanoate molecules results in similar adsorption energy per molecule in presence or absence of $LaClCO_3$ molecules. These results indicate that lanthanum ions added prior to carboxylate collector act as chemical bridges between the monazite surface and the carboxylate collectors functional group, increasing the affinity of these latter for the mineral surface.

This new approach of using a soluble rare earth salt to improve the floatability of a REM may be regarded as irrelevant from an economic point of view. Nonetheless, the use of metal salts to activate or depress the adsorption of collectors on mineral surfaces is a widespread industrial practice in flotation, its economic sustainability being assured if the required dosage of metal salts is reduced. Overall, this study is the first step towards the development of a new approach in the flotation of monazite for REE extraction: soluble lanthanum salts exhibit significant synergistic effects with carboxylate collectors and could therefore be used as a promoter to increase the REE recovery from low grades, fine-grained, or complex ores. The results and the methodology presented in this study promise tangible progress on the selective recovery of monazite throughout flotation operations though it could be applied to most non-metal ores processed by flotation nowadays.

5. Acknowledgements

This research was funded by the Carnot Institutes ICEEL and BRGM through the TERRAFINE Inter-Carnot Action (Carnot-ICEEL no. 118-IC and IC-BRGM no. 2013-01). Financial support from LabEx RESSOURCES21 is also acknowledged (contract Investissements d'Avenir no. ANR–10–LABX–0021). This work was granted access to the HPC resources of TGCC and CINES under the allocation 2019-A0060910433 made by GENCI. The authors would like to thank Martine Mallet (LCPME, UMR 7564 CNRS - University of Lorraine) for fruitful discussion and comments on the XPS analyses and Hubert Haas (BRGM) for providing the equipment required for thermal treatment of monazite precursors.

6. References

[1] S.C. Chelgani, M. Rudolph, T. Leistner, J. Gutzmer, U.A. Peuker, A review of rare earth minerals flotation: monazite and xenotime, Int. J. Min. Sci. Technol. 25 (2015) 877–883. https://doi.org/10.1016/j.ijmst.2015.09.002.

[2] R. Houot, J.-P. Cuif, Y. Mottot, J.-C. Samama, Recovery of rare earth minerals, with emphasis on flotation process, Mater. Sci. Forum. 70–72 (1991) 301–324. https://doi.org/10.4028/www.scientific.net/MSF.70-72.301.

[3] A. Jordens, Y.P. Cheng, K.E. Waters, A review of the beneficiation of rare earth element bearing minerals, Miner. Eng. 41 (2013) 97–114. https://doi.org/10.1016/j.mineng.2012.10.017.

[4] C. Tunsu, Y. Menard, D.Ø. Eriksen, C. Ekberg, M. Petranikova, Recovery of critical materials from mine tailings: A comparative study of the solvent extraction of rare earths using acidic, solvating and mixed extractant systems, J. Clean. Prod. 218 (2019) 425–437. https://doi.org/10.1016/j.jclepro.2019.01.312.

[5] S. Peelman, Z.H.I. Sun, J. Sietsma, Y. Yang, Hydrometallurgical Extraction of Rare Earth Elements from Low Grade Mine Tailings, in: S. Alam, H. Kim, N.R. Neelameggham, T. Ouchi, H. Oosterhof (Eds.), Rare Met. Technol. 2016, Springer International Publishing, Cham, 2016: pp. 17–29. https://doi.org/10.1007/978-3-319-48135-7_2.

[6] G.B. Abaka-Wood, M. Zanin, J. Addai-Mensah, W. Skinner, The upgrading of rare earth oxides from iron-oxide silicate rich tailings: Flotation performance using sodium oleate and hydroxamic acid as collectors, Adv. Powder Technol. 29 (2018) 3163–3172. https://doi.org/10.1016/j.apt.2018.08.019.

[7] Q. Dehaine, L.O. Filippov, H.J. Glass, G. Rollinson, Rare-metal granites as a potential source of critical metals: A geometallurgical case study, Ore Geol. Rev. 104 (2019) 384–402. https://doi.org/10.1016/j.oregeorev.2018.11.012.

[8] E.R.L. Espiritu, G.R. Da Silva, D. Azizi, F. Larachi, K.E. Waters, Flotation behavior and electronic simulations of rare earth minerals in the presence of dolomite supernatant using sodium oleate collector, J. Rare Earths. 37 (2019) 101–112. https://doi.org/10.1016/j.jre.2018.04.016.

[9] Q. Meng, Z. Yuan, L. Yu, Y. Xu, Y. Du, Study on the activation mechanism of lead ions in the flotation of ilmenite using benzyl hydroxamic acid as collector, J. Ind. Eng. Chem. 62 (2018) 209–216. https://doi.org/10.1016/j.jiec.2017.12.059.
[10] J. Ren, S. Song, A. Lopez-Valdivieso, S. Lu, Selective flotation of bastnaesite from monazite in rare earth concentrates using potassium alum as depressant, Int. J. Miner. Process. 59 (2000) 237–245. https://doi.org/10.1016/S0301-7516(99)00075-7.
[11] L. Ren, H. Qiu, M. Zhang, K. Feng, P. Liu, J. Guo, J. Feng, Behavior of Lead Ions in Cassiterite Flotation Using Octanohydroxamic Acid, Ind. Eng. Chem. Res. 56 (2017) 8723–8728. https://doi.org/10.1021/acs.iecr.7b02126.
[12] Tian, Z. Gao, W. Sun, H. Han, L. Sun, Y. Hu, Activation role of lead ions in benzohydroxamic acid flotation of oxide minerals: New perspective and new practice, J. Colloid Interface Sci. 529 (2018) 150–160. https://doi.org/10.1016/j.jcis.2018.05.113.
[13] Tian, R. Liu, Z. Gao, P. Chen, H. Han, L. Wang, C. Zhang, W. Sun, Y. Hu, Activation mechanism of Fe (III) ions in cassiterite flotation with benzohydroxamic acid collector, Miner. Eng. 119 (2018) 31–37. https://doi.org/10.1016/j.mineng.2018.01.011.
[14] L. Xia, B. Hart, B. Loshusan, A Tof-SIMS analysis of the effect of lead nitrate on rare earth flotation, Miner. Eng. 70 (2015) 119–129. https://doi.org/10.1016/j.mineng.2014.09.008.
[15] W. Xiao, P. Cao, Q. Liang, X. Huang, K. Li, Y. Zhang, W. Qin, G. Qiu, J. Wang, Adsorption behavior and mechanism of Bi(III) ions on rutile–water interface in the presence of nonyl hydroxamic acid, Trans. Nonferrous Met. Soc. China. 28 (2018) 348–355. https://doi.org/10.1016/S1003-6326(18)64668-0.
[16] J. He, H. Han, C. Zhang, Z. Xu, D. Yuan, P. Chen, W. Sun, Y. Hu, Novel insights into the surface microstructures of lead(II) benzohydroxamic on oxide mineral, Appl. Surf. Sci. 458 (2018) 405–412. https://doi.org/10.1016/j.apsusc.2018.07.085.
[17] A. Jordens, C. Marion, T. Grammatikopoulos, B. Hart, K.E. Waters, Beneficiation of the Nechalacho rare earth deposit: Flotation response using benzohydroxamic acid, Miner. Eng. 99 (2016) 158–169. https://doi.org/10.1016/j.mineng.2016.08.024.
[18] C.F.F. Lopes, K. Iha, E.A. Neves, M.E.V. Suárez-Iha, A comparison of carboxylate complexes of Lanthanum (III): formate, acetate and propionate, J. Coord. Chem. 40 (2006) 27–34. https://doi.org/10.1080/00958979608022843.
[19] R. Janicki, A. Mondry, P. Starynowicz, Carboxylates of rare earth elements, Coord. Chem. Rev. 340 (2017) 98–133. https://doi.org/10.1016/j.ccr.2016.12.001.
[20] J. Lu, R. Wang, Lanthanides: Carboxylates, in: R.A. Scott (Ed.), Encycl. Inorg. Bioinorg. Chem., John Wiley & Sons, Ltd, Chichester, UK, 2012. https://doi.org/10.1002/9781119951438.eibc2024.
[21] R. Wang, Z. Zheng, Rare Earth Complexes with Carboxylic Acids, Polyaminopolycarboxylic Acids, and Amino Acids, in: C. Huang (Ed.), Rare Earth Coord. Chem., John Wiley & Sons, Ltd, Chichester, UK, 2010: pp. 91–136. https://doi.org/10.1002/9780470824870.ch3.
[22] K. Ohto, M. Yano, K. Inoue, T. Yamamoto, M. Goto, F. Nakashio, S. Shinkai, T. Nagasaki, Solvent Extraction of Trivalent Rare Earth Metal Ions with Carboxylate Derivatives of Calixarenes., Anal. Sci. 11 (1995) 893–902. https://doi.org/10.2116/analsci.11.893.
[23] A.C. du Preez, J. S Preston, The solvent extraction of rare-earth metals by carboxylic acids, Solvent Extr. Ion Exch. 10 (1992) 207–230. https://doi.org/10.1080/07366299208918101.
[24] F. Xie, T.A. Zhang, D. Dreisinger, F. Doyle, A critical review on solvent extraction of rare earths from aqueous solutions, Miner. Eng. 56 (2014) 10–28. https://doi.org/10.1016/j.mineng.2013.10.021.

[25] Q. Zhou, H. Yang, C. Yan, W. Luo, X. Li, J. Zhao, Synthesis of carboxylic acid functionalized diatomite with a micro-villous surface via UV-induced graft polymerization and its adsorption properties for Lanthanum(III) ions, Colloids Surf. Physicochem. Eng. Asp. 501 (2016) 9–16. https://doi.org/10.1016/j.colsurfa.2016.04.030.
[26] R. Arnold, L.B.S. Hing, Selectivity of carboxylic ion-exchange resin for lanthanide ions, J. Chem. Soc. Inorg. Phys. Theor. (1967) 306. https://doi.org/10.1039/j19670000306.
[27] D. Brancaccio, M. Cozzolino, Lanthanum carbonate: Time to abandon prejudices?, Kidney Int. 71 (2007) 190–192. https://doi.org/10.1038/sj.ki.5002079.
[28] R. Denkewicz, E. Senderov, J. Grenier, T. Souza, Lanthanide halide water treatment compositions and methods, US6312604B1, 2001. https://patentimages.storage.googleapis.com/63/c0/67/a87609f66f7a87/US6312604.pdf.
[29] S.A. Hannah, Phosphate Removal from Wastewaters using Lanthanum Precipitation, U.S. Department of the Interior - Federal Water Quality Administration, Cincinnati, Ohio, 1970.
[30] D. Mills, Removal of phosphate from water, US20050072740A1, 2005. https://patentimages.storage.googleapis.com/40/be/53/d3603812224526/US6846432.pdf.
[31] M. Ohno, H. Ohashi, H. Oda, H. Yokoyama, M. Okada, M. Nagaya, K. Izumi, H. Ito, S. Katoh, Lanthanum Carbonate for Hyperphosphatemia in Patients on Peritoneal Dialysis, Perit. Dial. Int. 33 (2013) 297–303. https://doi.org/10.3747/pdi.2012.00600.
[32] L. Fang, Q. Shi, J. Nguyen, B. Wu, Z. Wang, I.M.C. Lo, Removal Mechanisms of Phosphate by Lanthanum Hydroxide Nanorods: Investigations using EXAFS, ATR-FTIR, DFT, and Surface Complexation Modeling Approaches, Environ. Sci. Technol. 51 (2017) 12377–12384. https://doi.org/10.1021/acs.est.7b03803.
[33] J. Xie, Z. Wang, S. Lu, D. Wu, Z. Zhang, H. Kong, Removal and recovery of phosphate from water by lanthanum hydroxide materials, Chem. Eng. J. 254 (2014) 163–170. https://doi.org/10.1016/j.cej.2014.05.113.
[34] K. Reitzel, F.Ø. Andersen, S. Egemose, H.S. Jensen, Phosphate adsorption by lanthanum modified bentonite clay in fresh and brackish water, Water Res. 47 (2013) 2787–2796. https://doi.org/10.1016/j.watres.2013.02.051.
[35] X.-Z. Yuan, G. Pan, H. Chen, B.-H. Tian, Phosphorus fixation in lake sediments using LaCl3-modified clays, Ecol. Eng. 35 (2009) 1599–1602. https://doi.org/10.1016/j.ecoleng.2008.08.002.
[36] Y. He, H. Lin, Y. Dong, L. Wang, Preferable adsorption of phosphate using lanthanum-incorporated porous zeolite: Characteristics and mechanism, Appl. Surf. Sci. 426 (2017) 995–1004. https://doi.org/10.1016/j.apsusc.2017.07.272.
[37] Y. Foucaud, M. Badawi, L.O. Filippov, O. Barres, I.V. Filippova, S. Lebègue, Synergistic adsorptions of Na_2CO_3 and Na_2SiO_3 on calcium minerals revealed by spectroscopic and *ab initio* molecular dynamics studies, Chem. Sci. 10 (2019) 9928–9940. https://doi.org/10.1039/C9SC03366A.
[38] H. Jabraoui, E.P. Hessou, S. Chibani, L. Cantrel, S. Lebègue, M. Badawi, Adsorption of volatile organic and iodine compounds over silver-exchanged mordenites: A comparative periodic DFT study for several silver loadings, Appl. Surf. Sci. 485 (2019) 56–63. https://doi.org/10.1016/j.apsusc.2019.03.282.
[39] Y. Berro, S. Gueddida, S. Lebègue, A. Pasc, N. Canilho, M. Kassir, F.E.H. Hassan, M. Badawi, Atomistic description of phenol, CO and H2O adsorption over crystalline and amorphous silica surfaces for hydrodeoxygenation applications, Appl. Surf. Sci. 494 (2019) 721–730. https://doi.org/10.1016/j.apsusc.2019.07.216.
[40] C. Peng, Y. Zhong, G. Wang, F. Min, L. Qin, Atomic-level insights into the adsorption of rare earth Y(OH)3-nn+ (n = 1–3) ions on kaolinite surface, Appl. Surf. Sci. 469 (2019) 357–367. https://doi.org/10.1016/j.apsusc.2018.11.022.

[41] Y. Foucaud, M. Badawi, L. Filippov, I. Filippova, S. Lebègue, A review of atomistic simulation methods for surface physical-chemistry phenomena applied to froth flotation, Miner. Eng. 143 (2019) 106020. https://doi.org/10.1016/j.mineng.2019.106020.
[42] A. Sarvaramini, D. Azizi, F. Larachi, Hydroxamic acid interactions with solvated cerium hydroxides in the flotation of monazite and bastnäsite—Experiments and DFT study, Appl. Surf. Sci. 387 (2016) 986–995. https://doi.org/10.1016/j.apsusc.2016.07.044.
[43] A. Geneyton, L.O. Filippov, N.E. Menad, Effects of atom substitutions and dissolved carbonate species on monazite electrophoretic mobility, Colloids Surf. Physicochem. Eng. Asp. 570 (2019) 141–146. https://doi.org/10.1016/j.colsurfa.2019.03.005.
[44] J. Gamage McEvoy, Y. Thibault, Impact of crystal chemistry properties on the collector-mineral interactions observed for REE orthophosphates and oxides, Appl. Surf. Sci. 466 (2019) 970–981. https://doi.org/10.1016/j.apsusc.2018.10.103.
[45] D.A. Shirley, High-Resolution X-Ray Photoemission Spectrum of the Valence Bands of Gold, Phys. Rev. B. 5 (1972) 4709–4714. https://doi.org/10.1103/PhysRevB.5.4709.
[46] G. Kresse, J. Hafner, *Ab initio* molecular dynamics for liquid metals, Phys. Rev. B. 47 (1993) 558–561. https://doi.org/10.1103/PhysRevB.47.558.
[47] P.E. Blöchl, Projector augmented-wave method, Phys. Rev. B. 50 (1994) 17953–17979. https://doi.org/10.1103/PhysRevB.50.17953.
[48] G. Kresse, D. Joubert, From ultrasoft pseudopotentials to the projector augmented-wave method, Phys. Rev. B. 59 (1999) 1758–1775. https://doi.org/10.1103/PhysRevB.59.1758.
[49] J.P. Perdew, K. Burke, M. Ernzerhof, Generalized Gradient Approximation Made Simple, Phys. Rev. Lett. 77 (1996) 3865–3868. https://doi.org/10.1103/PhysRevLett.77.3865.
[50] S. Grimme, Semiempirical GGA-type density functional constructed with a long-range dispersion correction, J. Comput. Chem. 27 (2006) 1787–1799. https://doi.org/10.1002/jcc.20495.
[51] W. Kohn, L.J. Sham, Self-Consistent Equations Including Exchange and Correlation Effects, Phys. Rev. 140 (1965) A1133–A1138. https://doi.org/10.1103/PhysRev.140.A1133.
[52] G. Kresse, J. Furthmüller, Efficient iterative schemes for *ab initio* total-energy calculations using a plane-wave basis set, Phys. Rev. B. 54 (1996) 11169–11186. https://doi.org/10.1103/PhysRevB.54.11169.
[53] Y. Ni, J.M. Hughes, A.N. Mariano, Crystal chemistry of the monazite and xenotime structures, Am. Mineral. 80 (1995) 21–26. https://doi.org/10.2138/am-1995-1-203.
[54] J.W. Anthony, R.A. Bideaux, K.W. Bladh, M.C. Nichols, Handbook of Mineralogy, Mineralogical Society of America, Chantilly, VA 20151-1110, USA, 2000. http://www.handbookofmineralogy.org/.
[55] W. Overstreet, The Geologic occurence of monazite, 1967.
[56] W. Zhang, R.Q. Honaker, J.G. Groppo, Flotation of monazite in the presence of calcite part I: Calcium ion effects on the adsorption of hydroxamic acid, Miner. Eng. 100 (2017) 40–48. https://doi.org/10.1016/j.mineng.2016.09.020.
[57] K. Momma, F. Izumi, *VESTA 3* for three-dimensional visualization of crystal, volumetric and morphology data, J. Appl. Crystallogr. 44 (2011) 1272–1276. https://doi.org/10.1107/S0021889811038970.
[58] A. Geneyton, L.O. Filippov, A. Renard, M. Mallet, N.-E. Menad, Advances in carboxylate collectors adsorption on monazite surface: Part 1 – Assessment of the hydroxylation and carbonation of surface lanthanide ions, Appl. Surf. Sci. 485 (2019) 283–292. https://doi.org/10.1016/j.apsusc.2019.04.017.
[59] R.K. Lam, J.W. Smith, A.M. Rizzuto, O. Karslıoğlu, H. Bluhm, R.J. Saykally, Reversed interfacial fractionation of carbonate and bicarbonate evidenced by X-ray photoemission spectroscopy, J. Chem. Phys. 146 (2017) 094703. https://doi.org/10.1063/1.4977046.

[60] A. Shchukarev, D. Korolkov, XPS Study of group IA carbonates, Open Chem. 2 (2004). https://doi.org/10.2478/BF02475578.
[61] Y. Foucaud, S. Lebègue, L.O. Filippov, I.V. Filippova, M. Badawi, Molecular Insight into Fatty Acid Adsorption on Bare and Hydrated (111) Fluorite Surface, J. Phys. Chem. B. 122 (2018) 12403–12410. https://doi.org/10.1021/acs.jpcb.8b08969.
[62] Y. Foucaud, M. Badawi, L.O. Filippov, I.V. Filippova, S. Lebègue, Surface Properties of Fluorite in Presence of Water: An Atomistic Investigation, J. Phys. Chem. B. 122 (2018) 6829–6836. https://doi.org/10.1021/acs.jpcb.8b02717.
[63] N.H. de Leeuw, T.G. Cooper, The layering effect of water on the structure of scheelite, Phys. Chem. Chem. Phys. 5 (2003) 433–436. https://doi.org/10.1039/b210461j.
[64] W. Cui, X. Song, J. Chen, Y. Chen, Y. Li, C. Zhao, Adsorption Behaviors of Different Water Structures on the Fluorapatite (001) Surface: A DFT Study, Front. Mater. 7 (2020) 47. https://doi.org/10.3389/fmats.2020.00047.